JOURNAL OF GEOPHYSICAL RESEARCH, VOL. 108, NO. D13, 4388, doi:10.1029/2002JD002393, 2003

A yearlong comparison of plot-scale and satellite footprint-scale 19 and 37 GHz brightness of the Alaskan North Slope

E. J. Kim

Laboratory for Hydrospheric Processes, NASA Goddard Space Flight Center, Greenbelt, Maryland, USA

A. W. England

Department of Atmospheric, Oceanic, and Space Sciences and Department of Electrical Engineering and Computer Science, University of Michigan, Ann Arbor, Michigan, USA

Received 28 March 2002; revised 10 December 2002; accepted 24 February 2003; published 10 July 2003.

[1] Subpixel heterogeneity remains a key issue in the estimation of land parameters using satellite passive microwave sensors; the scales of spatial variability on land are typically much smaller than sensor footprints (tens of km). Disaggregation is a necessary component of any successful assimilation or retrieval scheme attempting to exploit satellite passive microwave observations to estimate parameters at the local scale. This paper quantifies the similarity between ground-based brightness and satellite brightness observations at 19 and 37 GHz for Arctic tundra on the North Slope of Alaska, identifying and quantifying sources of the differences. To the extent that this very homogeneous area represents a limiting case, the impact of subpixel heterogeneity in less homogeneous areas may be gauged. The ground-based radiobrightness observations were collected during the Radiobrightness Energy Balance Experiment 3 (REBEX-3) conducted on the North Slope in 1994–1995. A comparison was made of 381 days of brightness observations from a tower-mounted Special Sensor Microwave Imager (SSM/I) simulator representing the full range of annual conditions with coincident satellite SSM/I observations. Issues such as instrument stability, the effects of atmospheric radiative transfer, and consistency of satellite pixel locations are considered. Linear correlations between tower-based and SSM/I brightness observations of 0.93, 0.94, 0.93, and 0.92 were observed for the 19V, 19H, 37V, and 37H channels, respectively. Footprint sizes were 2×4 m for the tower-based observations and 43×69 km for the resampled SSM/I observations. Atmospheric, topographic, and time-of-observation effects can account for the differences between the best fit lines and the 1:1 lines, with calibration errors accounting for the residual differences. *INDEX TERMS:* 1823 Hydrology: Frozen ground; 1863 Hydrology: Snow and ice (1827); 3360 Meteorology and Atmospheric Dynamics: Remote sensing; 6969 Radio Science: Remote sensing; 9315 Information Related to Geographic Region: Arctic region; *KEYWORDS:* remote sensing, microwaves, radiometry, Arctic, tundra, land surface

Citation: Kim, E. J., and A. W. England, A yearlong comparison of plot-scale and satellite footprint-scale 19 and 37 GHz brightness of the Alaskan North Slope, *J. Geophys. Res.*, *108*(D13), 4388, doi:10.1029/2002JD002393, 2003.

1. Background

[2] The Arctic is a key component of both atmospheric and oceanic general circulations, through which Arctic processes interact with global processes. Several climate warming scenarios have predicted that the largest changes will occur at high latitudes [*Houghton et al.*, 1996]. For example, doubled-CO_2 atmospheric general circulation model simulations predict increases in the global mean surface air temperature of 1°–4.5°C by the year 2100 [*Houghton et al.*, 1996], with even greater warming expected in certain parts of the Arctic [*Manabe et al.*, 1991].

[3] Both short-term and long-term warming trends have already been observed in the Arctic [*Chapman and Walsh*, 1993; *Hansen and Lebedeff*, 1987]. Decadal or longer-term warming of permafrost is apparent in borehole temperature profiles [*Osterkamp and Romanovsky*, 1999; *Lachenbruch and Marshall*, 1986]; this has resulted in a loss of permafrost [*Williams and Smith*, 1989; *Houghton et al.*, 1996] and will result in changes in the regional ecosystems [*Oechel et al.*, 2000; *Michaelson et al.*, 1996]. Warming promotes thawing of the permafrost, which affects the surface hydrology of the Arctic through a deeper active layer (the upper portion of the tundra and permafrost which thaws

0148-0227/03/2002JD002393

during the summer), increased soil moisture storage, warmer soil temperatures, and increased evaporation [*Hinzman and Kane*, 1992].

[4] Arctic tundra, the most representative biome underlain by permafrost, covers ~5.4% of the Earth's land surface ($\approx 8 \times 10^6$ km^2) [*Schlesinger*, 1991]. Arctic tundra is an important source and sink of carbon dioxide and methane, globally important greenhouse gases. Studies by *Oechel et al.* [1993] and others indicate that during the 1990s the tundra of the Alaskan North Slope had been on the borderline between being a net carbon source and a net carbon sink. The uptake and release of carbon by the tundra are affected by soil moisture and temperature [*Oberbauer and Oechel*, 1989]. Climate warming could result in a net release of carbon in the form of greenhouse gases [*Oechel et al.*, 1993; *Oechel and Vourlitis*, 1995]. This is potentially quite significant since tundra vegetation and soils contain an estimated 7.2% (4×10^9 t) of the world's organic carbon [*Schlesinger*, 1991], and a recent study (C. Ping, unpublished data, 1996) suggests that an equivalent additional amount has not been included in such estimates because it lies just below the present-day maximum thaw depth.

[5] Land surface processes (LSPs) regulate the fluxes of radiant energy, sensible heat, latent heat, moisture, and momentum at the land-atmosphere boundary, determining the response of the land to atmospheric forcing and feedbacks to the atmosphere [*Trenberth*, 1992]. These processes are complex and interrelated. For example, melting snow decreases the albedo of the land surface, allowing more solar radiation to be absorbed. The warmer land leads to higher air temperatures, which can lead to further melting of snow cover in a positive feedback loop.

[6] A key tool for monitoring climate change would be a means of observing Arctic LSPs. The lack of adequate observational data has been repeatedly recognized as a serious impediment to climate model improvement [*Houghton et al.*, 1992, 1996]. This lack is particularly felt in remote areas, where observing stations are widely scattered [*Washburn and Weller*, 1986]. Because the vastness and inaccessibility of Arctic lands preclude a significant increase in the number of surface observing stations, satellite remote sensing may be the only practical and economical approach to uniform, frequent observations of climatological forcing and response variables at regular intervals and at useful spatial resolutions [*Sellers*, 1992].

[7] There are numerous polar-orbiting platforms providing excellent spatial and temporal coverage of high-latitude regions. Microwave remote sensing offers advantages that are especially well suited to the observation of these regions. Microwave sensors (active and passive) are far less susceptible to interference by clouds than are optical or infrared sensors, and they do not depend on solar illumination, permitting observations at night and throughout the long polar winter.

[8] Microwave radiometry is particularly sensitive to temperature and moisture distributions in vegetation canopies and in the underlying soil, while not exhibiting radar's sensitivity to vegetation structure and limitations on vegetation column density [*Dubois et al.*, 1995]. For example, direct sensing of near-surface soil moisture is possible through vegetation with column densities up to several kg m^{-2} [*Jackson et al.*, 1993] (versus 0.4 kg m^{-2} for radar), with lower frequencies (1–2 GHz) having greater "penetration." While no such low-frequency satellite radiometers are currently operational (the satellite Advanced Microwave Scanning Radiometer (AMSR) includes 10 and 6 GHz radiometers; there are also proposals to fly 1.4 GHz satellite radiometers in the next 5–10 years), higher-frequency radiometers such as the Special Sensor Microwave Imager (SSM/I) instruments have been operational since 1987 aboard the Sun-synchronous polar-orbiting U.S. Defense Meteorological Satellite Program (DMSP) satellites. Each makes typically four passes per day over points on the North Slope of Alaska (68°–72°N latitude). There are typically two operational satellites in orbit with staggered overflight times making continuous radiobrightness observations at 19, 22, 37, and 85 GHz. It is worth noting that while the spatial resolution of current passive microwave satellite sensors (tens of km) is not as good as that of satellite radar instruments or visible-light sensors (km or subkm), the resolution is comparable to that of current climate models, which employ grid cells having areas of hundreds to thousands of square kilometers in area [*Seth*, 1995].

[9] Earlier work for grass canopies (3 kg m^{-2}) showed that under all but quite dry conditions, at the SSM/I frequencies, the majority of observed emission comes from the vegetation and not from the underlying soil [*England and Galantowicz*, 1995; *Kim and England*, 1995]. Thus single observations alone (as opposed to a time series) provide very little information on soil temperature and moisture, and direct inversion is not a robust method for estimating these quantities. Even in cases where single observations can be directly inverted to estimate one quantity (e.g., 1.4 GHz brightness and near-surface soil moisture), inversion of other quantities (e.g., a moisture profile or latent heat flux) is not practical.

[10] Since radiobrightness is an integrated quantity, it is not unique. Different vertical profiles of temperature and moisture can produce the same radiobrightness. A specific forcing history and information about the particular soil and vegetation under observation can constrain the problem if the observations are available in a sufficiently dense time series. Deviations between predicted and observed radiobrightnesses would be used to "nudge," or correct, the model state, much as current operational numerical weather prediction models routinely assimilate remotely sensed and in situ observations through such techniques [*Schmugge and Andre*, 1991]. In general, the shorter the temporal interval between observations, the smaller the corrections needed.

[11] By assimilating passive microwave observations made over a period of time to constrain the model, surface fluxes (e.g., latent and sensible heat) as well as near-surface and subsurface temperature and moisture conditions will be determinable for areas with relatively thin vegetation, such as tundra and prairie. That is, the assimilation of satellite observations will permit regular wide-scale estimates to be made with a spatial resolution comparable to the sensor footprint. Again, these estimates would come from the model state, not from a direct inversion of radiobrightness data.

[12] One critical issue is that of subpixel variability within the footprint of a satellite radiometer, i.e., a scaling issue. Model validation is typically done at the (homogeneous) plot scale, yet satellite radiometer pixels are typically tens of kilometers in diameter. Presumably, the more similar these observations are, the greater the chance of success of an assimilation strategy. The Radiobrightness Energy Balance Experiment 3 (REBEX-3) was designed, among other objectives, to provide an assessment of this similarity for a case which should be ideal in many respects: the wide-open tundra expanses of the North Slope of Alaska.

[13] The degree of match is a measure of how well passive microwave satellite observations might be used to estimate surface conditions in such tundra/permafrost areas. In this paper we present quantitative answers to the questions, Specifically, how well do ground-based radiobrightness observations match satellite radiobrightness observations? What comparison issues exist (to what are the differences due?), and how might they affect such estimates?

[14] Section 2 describes the collection of ground-based observations and the preparation of satellite observations used to perform a comparison. These data are then presented and compared, and the results of the comparison are analyzed to highlight similarities and to identify the sources of the differences.

2. Methods and Materials

[15] Two types of data were used in our study: satellite microwave brightness observations and ground-based observations of microwave brightness and micrometeorological quantities. The ground-based observations (their purpose, location, and timing and details of the equipment used) will be described first, followed by details of the satellite data processing necessary for the comparison.

2.1. Ground-Based Data Collection

[16] REBEX-3 provides a unique set of long-term colocated microwave brightness and micrometeorological observations (1) to enable comparisons of contemporaneous ground-based and satellite brightness observations and (2) to calibrate future LSP models of tundra. Measured quantities included ground and sky microwave brightnesses at the SSM/I frequencies of 19.35 and 37.0 GHz (horizontal and vertical polarizations) and at 85.5 GHz (vertical polarization), the thermal infrared ground brightness, the net radiation, the upwelling and downwelling solar radiation, the Bowen ratio, soil moisture and soil temperature profiles, the soil heat flow, the air temperature, the relative humidity, wind speed and direction, liquid precipitation, snow depth, and the snow temperature profile. The subject of this paper is the scale comparison in objective 1. The land surface process modeling in objective 2 will be the subject of a future paper.

[17] The REBEX-3 data were collected using the Tower Mounted Radiometer System 2 (TMRS2). The TMRS2 was a ground-based SSM/I simulator and surface energy balance monitoring system designed and built at the University of Michigan. The TMRS series of instruments are used to collect long-term (months) time series data sets at sites representative of various biomes in support of land surface process modeling and remote sensing research. The TMRS2 was environmentally hardened for the Arctic and was designed to operate autonomously with remote monitoring and control capabilities via a low-bandwidth communications link such as a typical long-distance voice telephone channel. For REBEX-3, TMRS2 was deployed on the North Slope of Alaska in September 1994 at the time of maximum active layer thaw depth, necessary to emplace the subsurface sensors (temperature and moisture probes) in a tundra/permafrost environment. Observations were made through the 1994–1995 Arctic winter and through the summer of 1995. REBEX-3 was completed in September 1995.

Table 1. TMRS2 Radiometer Specifications[a]

Parameter	Value		
	Radiometer 1	Radiometer 2	Radiometer 3
Center frequency, GHz	19.35	37.0	85.5
Polarizations	H,V	H,V	V
IF bandwidth, MHz	10–250	100–1000	100–1500
Postdetection bandwidth, kHz	20	20	20
Integration time, s	1–2	1–2	1–2
Receiver self-noise T_{REC}, K	840	1280	3270
$NE\Delta T$, K	0.05	0.04	0.07
Antenna 3dB beamwidth, deg	10	10	10

[a] $NE\Delta T$ values assume a 300 K antenna temperature, a 1 s integration time, and gain variations $\Delta G/G = 10^{-5}$.

[18] The TMRS2 microwave radiometers operated in total power mode. They were installed in a heated, weatherproofed enclosure on top of a 10 m tower and observed the ground at the SSM/I incidence angle of 53° off nadir; the radiometer footprint was 2 × 4 m. Radiometer specifications are listed in Table 1, and a close-up photograph is shown in Figure 1.

[19] The TMRS2 radiometers were thermally controlled to achieve long-term stability in the harsh Arctic environment. The temperatures of the internal calibration reference (a waveguide matched termination) in each radiometer were stabilized to 0.2 K. This removed temperature-dependent radiometer gain and offset variations as a source of serious error.

[20] All supporting equipment, including the computer used for instrument control and data logging, and the communications equipment were housed in a small, heated trailer located 30 m from the radiometer tower. A radiotelephone link provided remote monitoring and control. Data could be downloaded, and control software could be maintained remotely from Michigan throughout the year, enormously facilitating the experiment.

[21] The REBEX-3 site was chosen to satisfy three basic requirements. First, the site had to be located within a continuous permafrost area, i.e., homogeneous land cover at the spatial resolution of SSM/I (~50 km after resampling), to simplify the comparison of ground-based and satellite microwave observations. "Continuous permafrost" refers to a contiguous area completely underlain by permafrost.

[22] Second, it was desirable to focus on sites which were inland from the coast and distant from mountains, again, because passive microwave satellite sensor footprints are large. The requirement to avoid the ocean and mountains would also simplify any future regional land surface process modeling. Logistical considerations constrained us to an

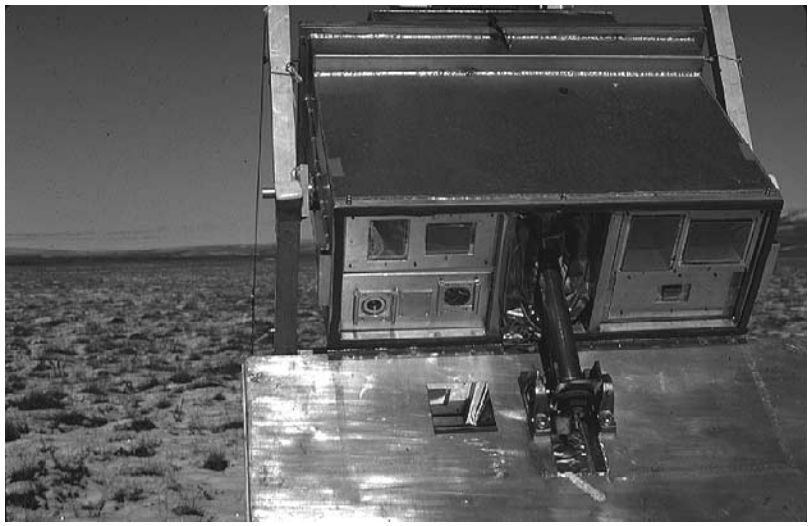

Figure 1. Close-up of the TMRS2 radiometer enclosure. Clockwise from top right are the 19 GHz H and V antennas; the 85 GHz V antenna; a video camera and the thermal IR radiometer; and the 37 GHz H and V antennas. Visible in the center area is a motorized actuator used to seal the housing between observations.

area nearly, but not completely, free of mountains. However, their effect was found to be small, as will be shown in section 3.2.

[23] Third, the site had to be a tundra area which had not been "disturbed" from its natural condition by proximity to roads, facilities, or human activities. Tundra 10–20 m away from a road typically showed no visual trace of disturbance. Logistical considerations constrained us to assume that locating our instruments 30 m away from the nearest disturbed tundra would sufficiently ensure "undisturbed" tundra for the purposes of REBEX-3.

[24] We were fortunate to obtain permission to use one of only two sites in the area which actually met the above three requirements: adjacent to the Alaska Department of Transportation (DOT) Saganavirktok (Sag) River Maintenance Camp (see Figure 2) on the North Slope at mile 306 on the Dalton Highway (the official name for the pipeline road). Details of land cover and soil are listed in Table 2. Through the use of a 330 m power cable, the TMRS2 instruments were located well away from the micrometeorological disturbances associated with the camp.

Figure 2. REBEX-3 site at Saganavirktok River, Alaska. The view is facing north along the pipeline road to Prudhoe Bay. The buildings on the right compose the Alaska Department of Transportation camp. The small white dot near the center of the image is the TMRS2 trailer. The distance across the center of the photo is 0.5 km.

[25] Beginning in the 1980s a number of researchers developed sites along the north-south transect of the Trans-Alaska Pipeline route. Examples of these efforts include the projects of Hinzman and Kane at Imnaviat Creek [*Hinzman et al.*, 1991; *Kane et al.*, 1990; *Hinzman and Kane*, 1992], the Long Term Ecological Research (LTER) Program at Toolik Lake [*Shaver*, 1995; *Chapin and Shaver*, 1985], and the Land-Atmosphere-Ice Interactions (LAII) Program of the U.S. National Science Foundation (of which this research was a part) [*Oechel et al.*, 1993; *Lynch et al.*, 1999]. More recent programs include the International Tundra Experiment (ITEX) [*Henry and Molau*, 1997] and the Cirmpolar Active-Layer Monitoring (CALM) program (information on CALM is available at http://k2.gissa.uc.edu/~kenhinke/CALM/). The Sag River DOT camp is 30 km north of ecological research sites in the Toolik Lake/Imnaviat Creek area and 50 km south of sites at Happy Valley (Figure 3), in a region along the pipeline transect where few other micrometeorological measurements suitable for model input were made. These distances

Table 2. REBEX-3 Site Details

Parameter	Details
Latitude, °N	68.76306
Longitude, °W	148.88194
Elevation, m	500
Slope/aspect	very flat
Soil	Pergelic Cryaquepts [*Michaelson et al.*, 1996]
Vegetation	moist acidic tussock tundra: sedges, mosses, lichens
Active layer depth, cm	50 maximum

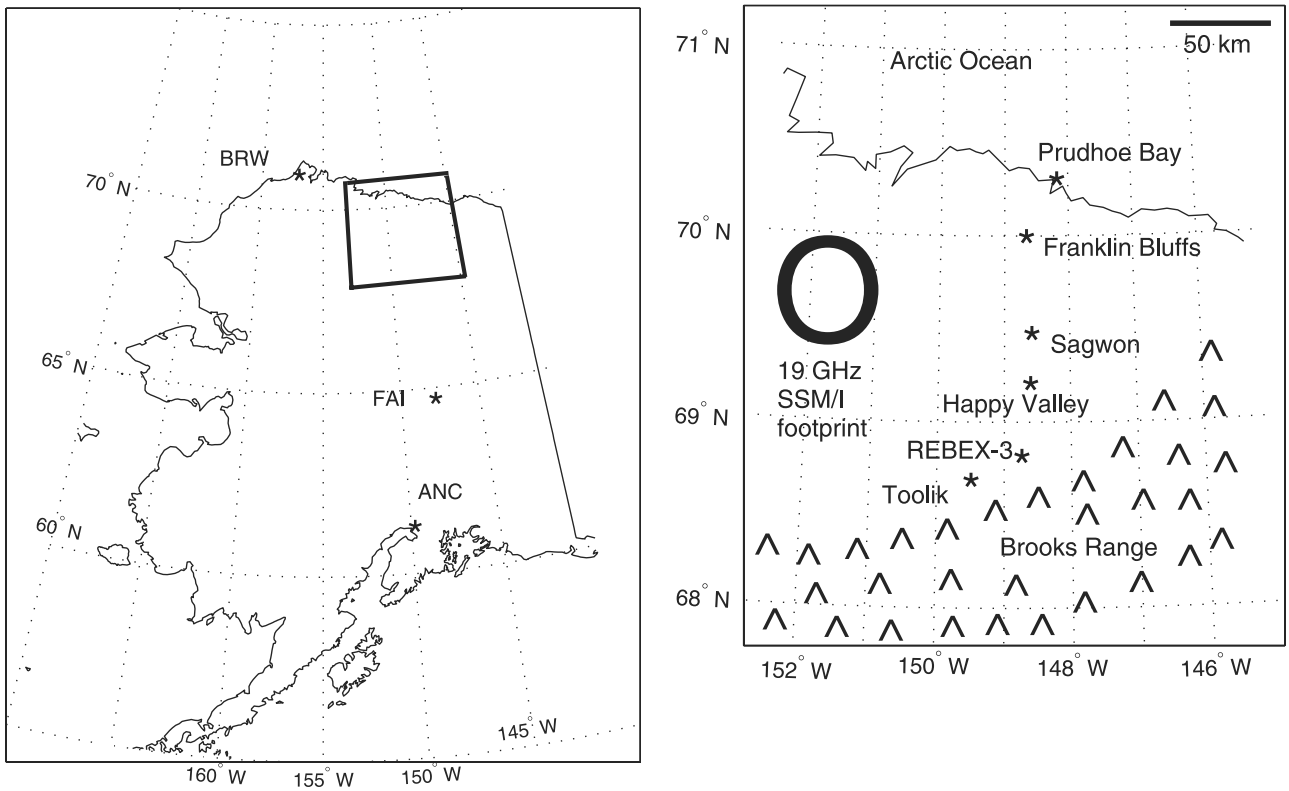

Figure 3. (left) REBEX-3 North Slope site location in Alaska. (right) Close-up of the REBEX-3 vicinity on the North Slope. An example 19 GHz SSM/I footprint is shown to scale.

are such that at scales of both the 20 km resolution of the mesoscale Arctic System Model (ARCSyM) [*Lynch et al.*, 1995] and the 25 km Equal Area Scalable Earth-Grid (EASE-Grid) (information on EASE-Grid is available at http://nsidc.org/data/ease/index.html) satellite data grid, a grid cell containing the REBEX-3 site would be between cells containing the Toolik/Imnaviat vicinity and the Happy Valley vicinity (see Figure 11 for an EASE-Grid map).

[26] Figure 4 shows snow-free conditions at the site. Figure 5 shows winter conditions at the site. Radiometer calibration and instrument maintenance visits were made in October 1994, January 1995, and April/May 1995.

2.2. Satellite Data Processing

[27] We now describe the processing of the satellite data used in the comparison. We shall begin with an overview of SSM/I instrument characteristics and DMSP satellite platform characteristics that are important for understanding the data preparation steps and the gridding technique, all of which affect the interpretation of the comparison.

[28] The Special Sensor Microwave Imager is a passive microwave imaging instrument which flies aboard Defense Meteorological Satellite Program (DMSP) platforms. SSM/I instruments have been making Earth observations since 1987 [*Hollinger et al.*, 1987]. A summary of relevant instrument and platform specifications is given in Tables 3 and 4 [*Hollinger et al.*, 1990; *Defense Meteorological Satellite Program*, 1995; *Hollinger et al.*, 1989].

[29] The DMSP satellites fly in Sun-synchronous polar orbits with staggered overflight times. Each completes 14.1 orbits per day, typically observing a given point on the Earth twice per day. Poleward of 55° latitude the SSM/I swaths overlap, except for a small region at each pole (poleward of 87.6°). For example, at the REBEX-3 latitude of ~69° each satellite typically makes 4 to 6 passes per day. These characteristics make the DMSP satellites excellent platforms for observing the Arctic.

[30] Three operational SSM/I instruments were in orbit during the REBEX-3 period aboard the F10, F11, and F13 DMSP satellites. The F10 satellite did not achieve the desired orbit. To avoid the effects of this "nonstandard" orbit on the spatial resampling and gridding process, F10 data were not used here.

[31] F11 and F13 SSM/I Temperature Data Record tapes were obtained from the Marshall Space Flight Center Distributed Active Archive Center (MSFC DAAC). F11 data were processed beginning with 1994 day 228 through 1995 day 273 (16 August 1994 to 30 September 1995). F13 data started to become available just before the REBEX-3 snow-free season in 1995. F13 data were processed beginning with 1995 day 123 through 1995 day 273 (3 May to 30 September 1995). REBEX-3 ground brightness data span the period from 1994 day 241 (29 August 1994) to 1995 day 257 (14 September 1995).

[32] While the conical scan geometry of SSM/I is convenient in that it provides observations made at a constant incidence angle and with pixels of constant size and shape, it does not generate a convenient coordinate system for pixels on the Earth's surface. Raw swath pixels fall along a series of circular arcs at regularly spaced intervals of 25 km for the non-85-GHz channels and at intervals of 12.5 km for the 85 GHz channels [*Hollinger et al.*, 1990].

Figure 4. Snow-free conditions, May 1995. Note the lumpy tussocks. The microwave and IR radiometers view the ground at the SSM/I viewing angle of 53° up from nadir.

[33] The actual swath pixel locations relative to a fixed location such as the REBEX-3 site are not constant on a daily or subdaily basis nor between the overlapping portions of two successive orbits. The standard DMSP orbit does have a repeat time of 16 days (interval between orbits with identical swath coverage), so swaths repeat to some level of accuracy. However, even for repeated swaths, the constituent pixel locations would differ along track. The use of data from multiple satellites further complicates matters. Nonstationary pixels represent an unwanted variable in any comparison of SSM/I and REBEX-3 ground data. The REBEX-3 site was within 20–30 km of the Brooks Range, so the combination of footprint size and nonstationary location could result in pixels "contaminated" with variable brightness contributions from mountains. Other nearby sites of future interest were within 10 km of the Arctic Ocean coastline with its potentially severe transition between water brightness values and land brightness values. Still other sites were located near transitions from the coastal plain to higher-elevation areas with different vegetation and moisture conditions.

Figure 5. Snow-covered conditions, January 1995. From left to right are the 1 m and 3 m tripods with micrometeorological instruments; the 10 m tower; and the communications antenna and control system trailer.

Table 3. Selected DMSP Satellite-Related SSM/I Specifications During REBEX-3 Prior to Resampling

	Satellite	
	F11	F13
Launch date	28 Nov. 1991	24 March 1995
Information as of	2 Sep. 1995	orbit 1276
Inclination, deg	98.8	98.8
Maximum altitude, km	851	856
Minimum altitude, km	844	844
Maximum swath width, km	1483	similar to F11
Minimum swath width, km	1414	similar to F11
Maximum incidence angle, deg	53.56	similar to F11
Minimum incidence angle, deg	53.16	similar to F11
Orbital period, min	101.9	102.0
Eccentricity	0.00129	0.00083
Ascending equator crossing, LT	1825	1743

[34] The solution to the problem of nonstationary pixels was to resample the SSM/I data from the swath reference frame to a fixed grid. The Equal-Area Scalable Earth Grid is a standard gridding scheme now used with a variety of data sets (M. J. Brodzik, EASE-Grid: A Versatile Set of Equal-Area Projections and Grids, National Snow and Ice Data Center, Boulder, CO, available on the World Wide Web at http://nsidc.org/data/ease/ease_grid.html), including SSM/I data, its original application. The SSM/I EASE-Grid is composed of (1) map projection definitions and a gridding scheme (K. W. Knowles, Points, pixels, grids, and cells-a mapping and gridding primer, National Snow and Ice Data Center, Boulder, CO, available on the World Wide Web at http://cires.colorado.edu/~knowlesk/ppgc.html) and (2) a specific method to interpolate SSM/I data from swath space to Earth-gridded coordinates. The two standard EASE-Grid projections are a polar azimuthal equal-area projection and a cylindrical equal-area projection. The latter is primarily

Table 4. Selected SSM/I Instrument-Related Specifications

			Effective Field of View, km			
Frequency, GHz	Polarization	Passband, MHz	Cross-Track	Along-Track	$NE\Delta T$, K	Integration Time, ms
19.35	V	10–250	43	69	0.43	7.95
19.35	H	10–250	43	69	0.41	7.95
22.235	V	10–250	40	60	0.67	7.95
37.0	V	100–1000	28	37	0.37	7.95
37.0	H	100–1000	29	37	0.37	7.95
85.5	V	100–1500	13	15	0.81	3.89
85.5	H	100–1500	13	15	0.74	3.89

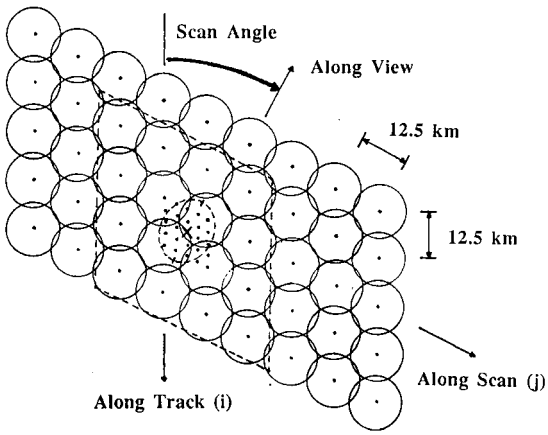

Figure 6. Portion of five consecutive scans. Circles represent raw swath pixels (note that actual footprints are not circles). Weighted brightness values from the 16 pixels within the dashed box are combined to generate interpolated observations on the densified grid. The dashed oval represents the footprint of the desired resampled observation, with a cross marking the center. The data from the nearest-neighbor pixel on the densified grid are reregistered to the EASE-Grid cell located at the cross. From *Galantowicz* [1995].

suited for studying midlatitude and low-latitude areas while the former is ideal for studying high-latitude and polar areas. All the projections are based on a spherical model of the Earth with radius R_E = 6371.228 km. The standard grid cell size is 25 × 25 km, but a 12.5 × 12.5 km cell size can also be used with data from the higher-resolution 85 GHz channels. Few cells have these exact dimensions, but all cells have the same area.

[35] The spatial interpolation scheme employed with the SSM/I EASE-Grid utilizes modified Backus-Gilbert optimal interpolation [*Backus and Gilbert*, 1970] based on the work of *Galantowicz and England* [1991], which, in turn, is based on the earlier work of *Poe* [1990] and *Stogryn* [1978]. The interpolation is optimal in the sense that an interpolated value for a particular location approximates the value which would have been obtained if the sensor had observed that location directly. A graphical depiction of EASE-Grid resampling is shown in Figure 6. An overview is presented in Appendix A, and a detailed description of the resampling technique has been given by *Galantowicz and England* [1991], *Galantowicz* [1995], and *Poe* [1990].

[36] A total of 3101 SSM/I orbit files from the F11 and F13 satellites were processed for the comparison studies in section 3. An example EASE-Grid image processed using the custom processor is shown in Figure 7.

3. Comparison and Discussion of Satellite and Ground Observations

[37] Given that the footprint of the REBEX-3 tower radiobrightness data was 2 × 4 m and that the footprint of the resampled and gridded SSM/I data is 43 × 69 km, it seems reasonable to limit the "analyses" to simple comparisons. More sophisticated analyses or "corrections" would require additional data on regional meteorological or surface conditions which were not available during REBEX-3 and which generally would not be available for such a remote area. For example, the location nearest the REBEX-3 site for which regular atmospheric sounding data are available is Barrow, Alaska, some 400 + km distant and located within a different (coastal) climate zone.

[38] To conduct a fair comparison of REBEX-3 ground radiobrightness data and SSM/I data, we must consider those sources which might reasonably be expected to contribute to any differences. The sources expected to be responsible for the largest differences include calibration errors and nonstationary pixel effects as well as atmospheric, scaling, and topographic effects. We will attempt to bound each of these effects in turn in order to arrive at a measure of how well the SSM/I data and the REBEX-3 ground data match.

[39] Yearlong time series of satellite brightnesses for the REBEX-3 cell and ground-based brightnesses from TMRS2 are presented in Figure 8. Figure 8 (top) shows $T_{B,\mathrm{EG}}$, the combined EASE-Grid brightnesses for F11 and F13 for the REBEX-3 cell (280,312), and Figure 8 (bottom) shows $T_{B,\mathrm{TMRS}}$, the TMRS2 tower brightness observations. Clearly, the two time series were very similar during the yearlong field experiment. In both cases the onset of snow accumulation is clearly marked by the divergence of the various channel brightnesses around day 250. The large fluctuations around days 475–510 (using the 1994 day-of-year to indicate 1995 days eliminates ambiguities) reflect the melting and refreezing of snow during snowmelt. These features are consistent with snowpack signatures reported in the literature [*Schanda et al.*, 1983; *Ulaby et al.*, 1986]. During

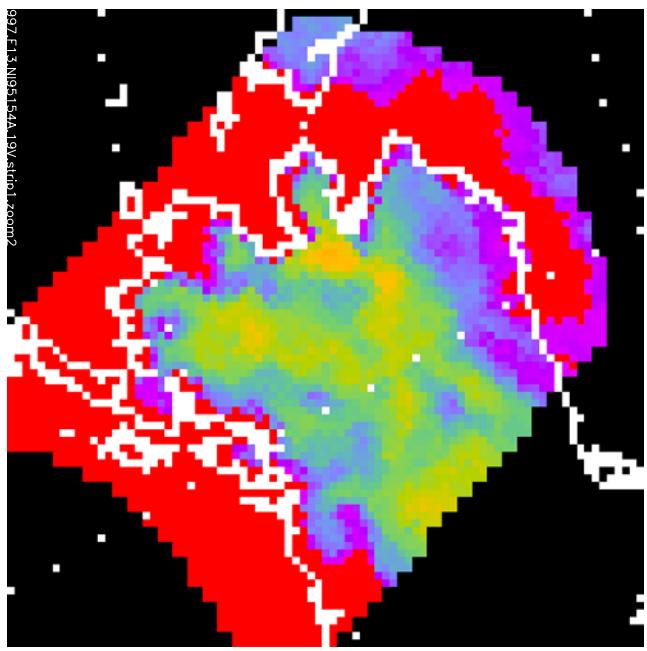

Figure 7. Example of custom EASE-Grid processor output zoomed to the region of interest. The image is from the F13 Defense Meteorological Satellite Program satellite with the 19V channel on 1995 day 154 during an ascending pass.

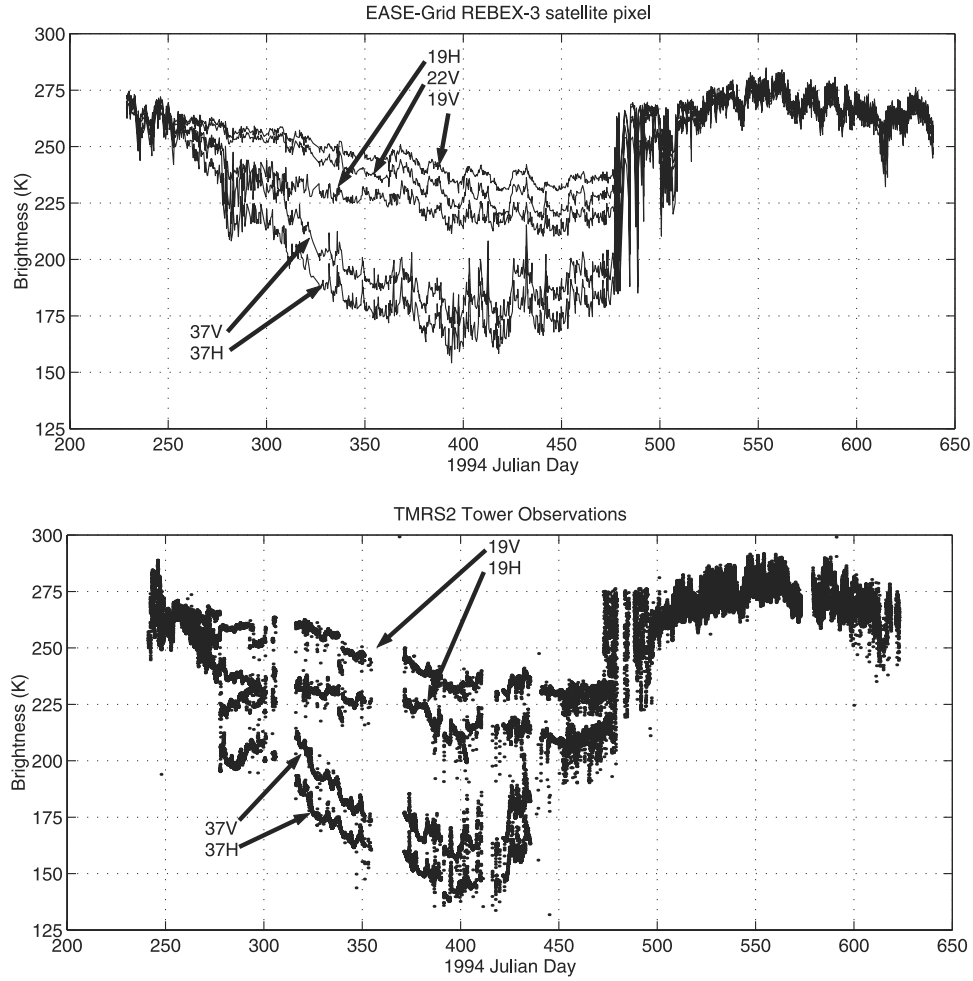

Figure 8. REBEX-3 SSM/I (EASE-Grid) and TMRS2 brightnesses with no adjustments, September 1994 to September 1995. (top) EASE-Grid 43 × 69 km footprint; from top to bottom, channels are 19V, 22V, 19H, 37V, and 37H. (bottom) TMRS2 2 × 4 m footprint: from top to bottom, channels are 19V, 19H, 37V, and 37H. The strong correlation indicates the potential utility of satellite microwave radiometry for monitoring surface conditions in a climatically sensitive tundra/permafrost area such as the North Slope. The transition from frozen to thawed surface conditions is clearly visible during days 475–510. Differences of a few days in the timing of melt at the REBEX-3 site versus across the pixel lead to the outliers visible in Figure 9. The colder 37 GHz brightnesses in Figure 8 (bottom) during days 275–475 are partly the result of the TMRS2 cold calibration error.

the snow-free period the distinguishing signature of snow-free tundra is the nearly equal brightnesses observed for all channels.

[40] Scatter diagrams of $T_{B,\mathrm{TMRS}}$ versus $T_{B,\mathrm{EG}}$ corresponding to the four paired channels shown in Figure 8 are shown in Figure 9. Least squares best fit and 1:1 lines are shown. The difference in $T_{B,\mathrm{TMRS}}$ (y axis difference) between the best fit line and the 1:1 line for $T_{B,\mathrm{EG}}$ (x axis) values of 77, 200, and 300 K for each channel is listed in Table 5. The high R^2 values indicate strong linear relationships and the closeness of the absolute match (closeness to the 1:1 line) before accounting for calibration errors or atmospheric or topographic effects. The outliers ($T_{B,\mathrm{TMRS}} \gg T_{B,\mathrm{EG}}$), most visible in Figure 9, represent times during snowmelt when the snow at the REBEX-3 site had melted several days before the snow across the whole EASE-Grid pixel. This early melt is typical for areas within 100–200 m of the pipeline road due to windblown road dust. The major results of our comparison are not affected by this local effect. The outliers are more pronounced for the 37 GHz channels than for the 19 GHz channels, as the 37 GHz response was generally more sensitive to snowpack conditions (as can be seen in Figure 8).

[41] The implications of such a strong linear relationship over the 4-order-of-magnitude difference in footprint sizes between the TMRS2 and SSM/I observations deserve some consideration. We know of no other examples of either a comparison or such a regular and consistent match between surface (or aircraft) and satellite passive microwave observations of the Earth's land surface over such a length of time (380 days). The causes of the small differences between $T_{B,\mathrm{TMRS}}$ and $T_{B,\mathrm{EG}}$ include differences in the exact times of the respective observations, the effect of mountains within the REBEX-3 EASE-Grid footprint, and atmospheric

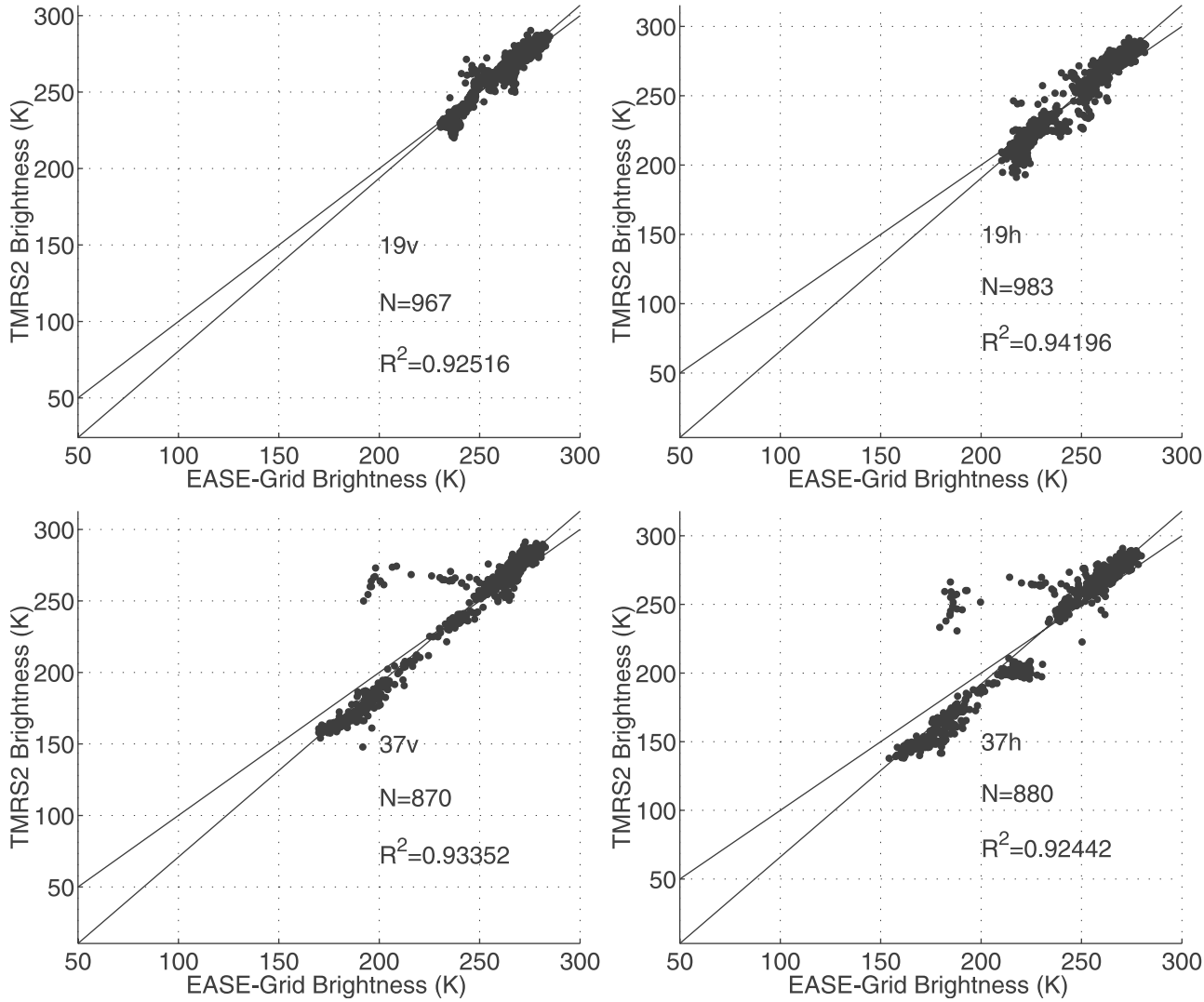

Figure 9. EASE-Grid versus TMRS2 brightnesses with no adjustments. The channels are (clockwise from top left) 19V, 19H, 37H, and 37V. Best linear fit and 1:1 lines are drawn. The outliers are due to differences of a few days in the timing of spring melt at the site versus across the pixel.

effects. We address each in sections 3.1, 3.2, and 3.3, respectively.

3.1. Time-of-Observation Differences

[42] Since TMRS2 observations were made every 30 min, the difference between the exact times of satellite and TMRS2 observations, Δt, was $\leq$15 min. The rate of change $dT_{B,\mathrm{TMRS}}(t)/dt$ had a mean magnitude of 1.5 K h^{-1}, but during times of maximum tundra heating or cooling, values of $\pm$12 K h^{-1} were not unusual (e.g., summertime tundra has a very low thermal mass), so up to $\pm$3 K of any difference in brightness values could be a result of time offsets of $\leq$15 min. The SSM/I overflights occurred during REBEX-3 local morning and late afternoon times (see Figure 10) when the ground brightnesses were often changing the fastest.

3.2. Topographic Effects

[43] On the North Slope in the vicinity of the REBEX-3 site the Brooks Range mountains and the tundra of the North Slope itself lie on either side of a fairly well-delineated boundary which runs approximately northeast-southwest for a distance spanning many EASE-Grid cells (Figure 11).

[44] The footprint size of an EASE-Grid pixel is the same as that of the 19V channel footprint, 69 km $\times$43 km. The

Table 5. EASE-Grid Satellite Versus TMRS2 Ground-Based Brightnesses[a]

	Brightness[b]		
Channel	77 K	200 K	300 K
19V	−22.4	−6.3	6.8
19H	−39.9	−9.5	15.2
37V	−33.9	−8.1	12.8
37H	−39.9	−8.0	17.9

[a]The values shown are the raw y axis differences (in K) between the best fit and 1:1 lines in Figure 9 for x axis values of 77, 200, and 300 K before any consideration of atmospheric, topographic, or calibration effects.

[b]The nominal cold calibration target temperature is 77 K, and the 200–300 K range spans summertime brightness values.

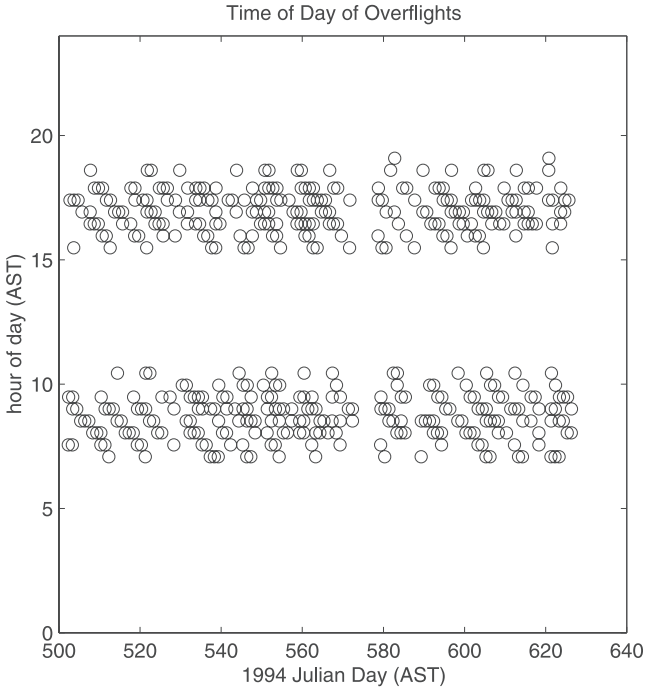

Figure 10. Typical SSM/I overflight times (F11 and F13 satellites). Abscissa spans the snow-free period. Alaska Standard Time (AST) = UTC − 9 hours.

REBEX-3 site was within 20 km of the northern edge of the Brooks Range mountains, so the footprint of the REBEX-3 EASE-Grid pixel included a portion of the mountains.

[45] The effect of mountains being included within the footprint of the REBEX-3 EASE-Grid pixel can be quantified in the following manner. We compared the signature of the REBEX-3 pixel to those from two nearby pixels: the nearest one whose footprint contained only mountains and the nearest one whose footprint contained only tundra. We will refer to these as the ''all-mountain'' and ''all-tundra'' pixels, respectively.

[46] The annual signatures of the 19 and 37 GHz channels are similar for all three pixels. The primary difference is that the all-mountain brightnesses are warmer during the winter and colder during the summer than are the brightnesses of the REBEX-3 pixel. Conversely, the all-tundra brightnesses are colder during the winter and warmer during the summer compared to the REBEX-3 pixel. We would expect the all-tundra brightnesses to match the TMRS2 brightnesses more closely than the all-mountain brightnesses, and they do.

[47] The effect of the mountains contaminating the REBEX-3 pixel was to introduce a warm error into the cold EASE-Grid brightnesses and a cold error into the hot EASE-Grid brightnesses. Thus in Figure 9, points at cold EASE-Grid brightness values should be adjusted to the left (toward colder values) while points at hot EASE-Grid brightness values should be adjusted to the right (toward hotter values) to more accurately reflect the tundra conditions at the REBEX-3 site. To quantify the adjustments, scatterplots were constructed to compare corresponding brightnesses for the REBEX-3 pixel and the all-tundra pixel. For each channel the adjustment to the best fit line necessary to match the 1:1 line in this scatter plot was taken as the correction necessary to remove the effects of the mountains in the scatter plots of Figure 9.

[48] The adjustment takes the form of a linear adjustment for each channel. Table 6 lists these horizontal adjustments to the best fit lines in Figure 9 at three discrete brightness values: 77, 200, and 300 K. The key result is that these amounts are small over the respective ranges of observed T_B values because the contamination occurred at the edge of the footprint where the gain of the synthetic antenna pattern was low.

3.3. Atmospheric Effects

[49] The effect of the atmosphere must be considered when comparing ground-based and satellite brightness observations at the SSM/I frequencies. This would be the case even if SSM/I and TMRS2 observed the exact same footprint on the ground, so it is not a spatial scaling problem per se; however, it is appropriate to include it in the current discussion. The atmosphere is a nonnegligible absorber and emitter of microwave radiation at 19 and 37 GHz.

[50] The total brightness seen by the SSM/I has three components: the actual brightness of the surface scene within the field of view of the instrument attentuated by the atmosphere, the upwelling ''sky'' brightness of the atmosphere itself, and the downwelling sky brightness reflected by the Earth's surface (the latter two in the

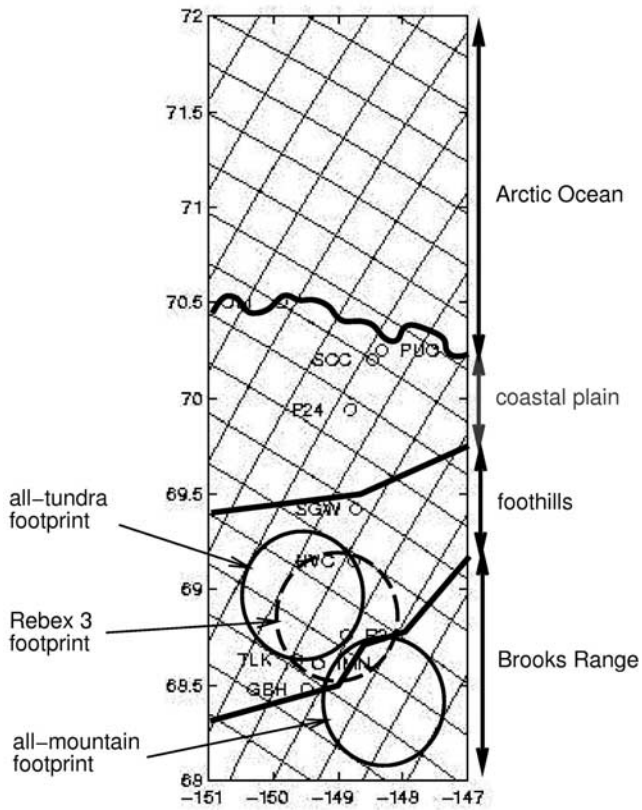

Figure 11. North Slope map with 25 km EASE-Grid overlay. The large circles represent EASE-Grid footprints. North is up. R3, REBEX-3 site; TLK, Toolik; IMN, Imnaviat; HVC, Happy Valley camp; GBH, Galbraith Lake; SGW, Sagwon Bluff; P24, Pipeline Mile 24; SCC, Deadhorse; PUO, Prudhoe Bay; OLI, Oliktok Point.

Table 6. Horizontal Brightness Temperature Adjustments to Figure 9 Best Fit Lines for Contamination by Mountains

	Brightness		
Channel	77 K	200 K	300 K
19V	−2.0	−0.3	1.1
19H	−9.4	−3.2	1.9
37V	−3.1	−0.8	1.0
37H	−5.5	−1.7	1.3

direction toward the instrument). A TMRS2 brightness, on the other hand, comprises two parts: actual surface brightness and reflected sky brightness.

[51] A "REBEX-3 standard atmosphere" and the standard radiative transfer model described by *Ulaby et al.* [1986] were used to compute the contribution of atmospheric absorption and emission at 19 and 37 GHz. No direct observations of cloud cover were made as part of REBEX-3, so for simplicity, we consider only the clear-sky case, accounting for absorption and emission by oxygen and water vapor. Furthermore, although average cloud cover for the eastern half of the North Slope is 55% [*Warren et al.*, 1986], the results of the cloud-free assumption do not indicate a significant effect. If warranted, a future study could estimate cloud conditions indirectly from other measurements.

[52] Microwave surface reflectivity was estimated by comparing REBEX-3 thermal infrared brightnesses and microwave brightnesses and by using the standard assumption that reflectivity equals one minus emissivity. We found that the snow-free reflectivity is small and nearly unpolarized, with a low value of ~0.04. Deviations from the true value would amount to only a second-order correction.

[53] The *U.S. Committee on Extension to the Standard Atmosphere* (*COESA*) [1966] defines 13 additional atmospheres at various latitudes and various seasons. Of relevance to REBEX-3 are the atmospheres for 60°N and 75°N, which bracket the REBEX-3 latitude. These are called "sub-Arctic" and "Arctic" by (*COESA*) [1966]. We refer to both as simply "Arctic." July, warm January, and cold January mean atmospheres are defined at these latitudes.

[54] The Arctic temperature profile has generally lower tropospheric temperatures and a lower tropopause (8–10 km versus 11 km, varying with season) than does the standard atmosphere, and there is a distinct surface temperature inversion during the winter. The thickness of the roughly isothermal portion of the stratosphere also increases with latitude. Taking averages of the 60°N and 75°N July profiles, we obtain the following approximate temperature profile for the "REBEX-3 standard atmosphere" for the summer season:

$$T(z) = T_0 - 6.5z \text{ K}, \qquad 0 \le z \le 10 \text{ km} \tag{1}$$

$$T(z) = T(10 \text{ km})\text{K}, \qquad 10 < z \le 30 \text{ km} \tag{2}$$

where T_0 is the temperature at sea level and z is height above sea level. The elevation of the REBEX-3 site was 0.5 km, so we replace equation (1) with $T(z) = (T_{\text{air}}) - 6.5(z-0.5)$, where T_{air} was the surface air temperature at the REBEX-3 site.

[55] Both the 60°N and 75°N July pressure profiles deviate from the *COESA* [1966] pressure profile by <1% below 10 km altitude [*COESA*, 1966]. We used the exponential approximation of *Ulaby et al.* [1986] (accurate to 3% below 10 km) to the *COESA* [1966] profile of pressure below 30 km, with surface pressure equal to 1013.25 hPa and a pressure scale height of 7.7 km.

[56] The water vapor density profile was approximated as it was by *Ulaby et al.* [1986], with an exponential expression with a scale height of 2 km. The surface water vapor density was computed using values of surface air temperature and relative humidity from REBEX-3 field data.

[57] While atmospheric absorption and emission are each as large as 25 K, the amounts are nearly equal so that the net effect (difference) is near zero over the 200-300 K range of summertime brightnesses (the period of primary interest). The difference between the atmospherically adjusted "surface" brightnesses, $T^*_{B,\text{EG}}$, and the original satellite values, $T_{B,\text{EG}}$, are shown in Figure 12. The plots show the amount to subtract from $T_{B,\text{EG}}$ to arrive at an adjusted brightness.

[58] Figure 12 indicates satellite brightnesses slightly greater than adjusted "surface" brightnesses, with a maximum adjustment of ~3 K. The effects of a clear atmosphere are small under the combination of surface brightnesses and atmospheric conditions considered. SSM/I can be an excellent observational tool under such conditions without requiring complex atmospheric corrections at 19 and 37 GHz. This is fortuitous for a region where meteorological observations are sparse.

3.4. Residual Differences

[59] We have compared ground-based brightness observations with colocated, contemporaneous satellite observations at 19 and 37 GHz, V and H polarizations. Very strong linear correlations ($R^2 > 0.92$) between SSM/I EASE-Grid and TMRS2 ground-based brightness observations were found for the 19 and 37 GHz SSM/I channels over the 380 day REBEX-3 period, even without adjusting for any atmospheric or topographic effects.

[60] So far, we have addressed three sources of the differences seen in Figure 9 and Table 5: the time of observations, topographic effects, and atmospheric effects. With respect to the scatter plots of Figure 9, the spread of the points about the best fit line is consistent with differences in the exact satellite and ground-based observation times. The best fit lines differ from the 1:1 lines by −22 to −40 K at $T_{B,\text{EG}} = 77$ K and by 6.8–17.9 K at $T_{B,\text{EG}} = 300$ K. Topographic effects were shown to shift $T_{B,\text{EG}}$ by up to −9.4 K at 77 K and by up to 1.9 K at 300 K. Atmospheric effects were shown to shift $T_{B,\text{EG}}$ by 6.8 K at 77 K and by up to −2.8 K at 300 K.

[61] The remaining differences were simply too consistently linear with respect to brightness to be attributable to natural phenomena. The data in Figure 9 span snow-free and snow-covered conditions, freeze-up and melt, day and night, hot and cold, wet and dry, and all atmospheric conditions over a full year. With such strong linear relationships in all four channels it is difficult to find plausible

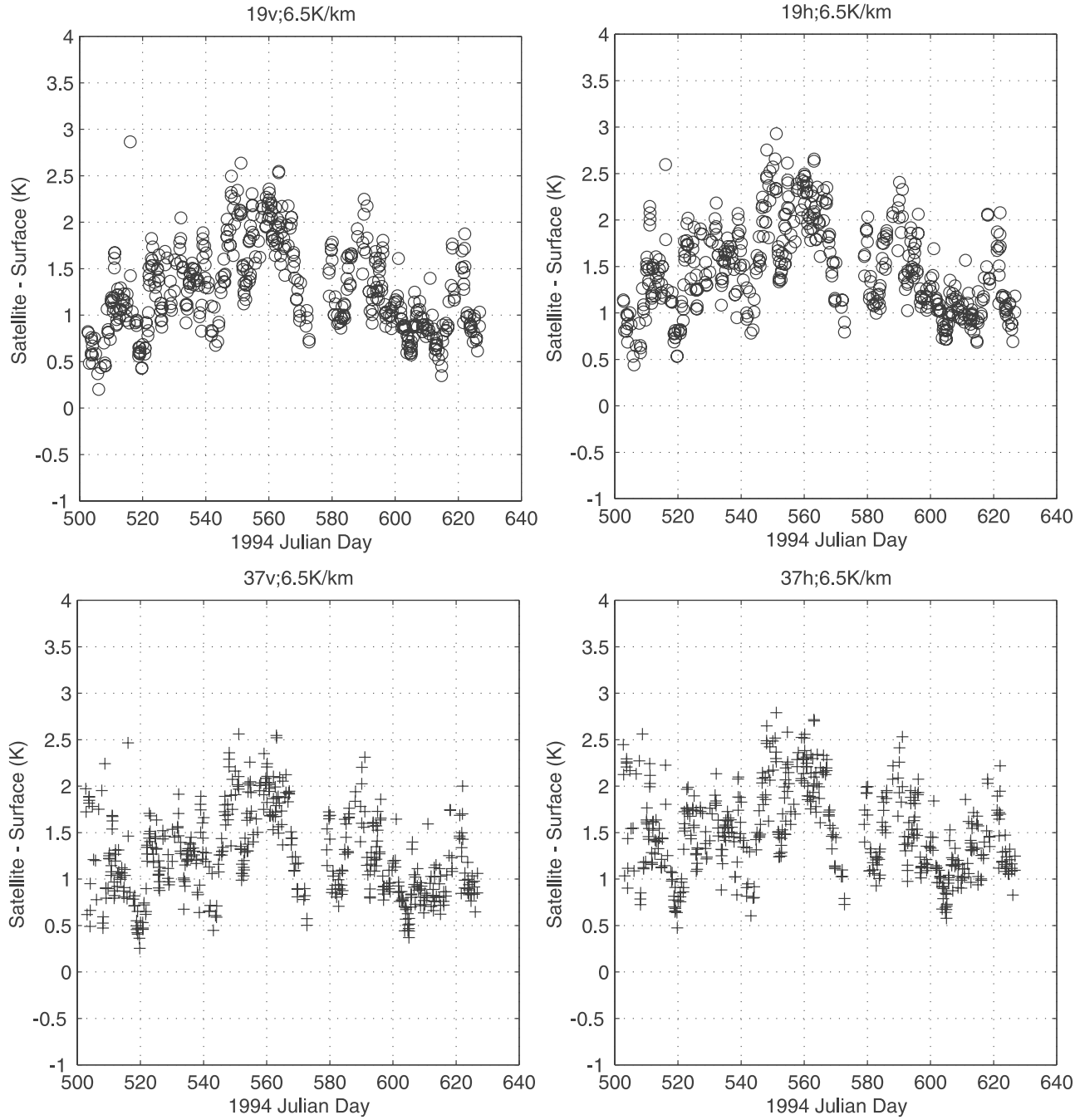

Figure 12. Atmospheric adjustments to EASE-Grid observations for the snow-free period.

explanations for anything other than an instrumentation-related cause.

[62] A number of instrumentation-related mechanisms were considered to explain the differences. In the end, only problems with the calibration target and the calibration procedure were plausible. Although the exact amount is not known, laboratory tests showed that up to 35–40 K of the difference between the 1:1 line and the best fit line at an abscissa value (EASE-Grid brightness) of 77 K can be explained by warm spots on the cold calibration target. We are confident that this cold calibration error accounts for the residual differences between the 1:1 and best fit lines for each channel. The high R^2 values found in the comparisons are based on relative relationships, which are unaffected by these absolute calibration problems.

4. Conclusions and Implications for Lower-Frequency Observations

[63] REBEX-3 was undertaken from September 1994 through September 1995 on the North Slope of Alaska. One of its purposes was to determine how well passive microwave satellite observations might be used to estimate surface conditions in tundra/permafrost areas. Specifically,

we sought to explore the scaling issue associated with large satellite radiometer footprints by determining how well ground-based radiobrightness observations would match satellite radiobrightness observations, to identify sources of any differences, and to begin to understand how they could affect estimates of surface conditions.

[64] The TMRS2 instrument system was developed for this project and was designed to collect the ground-based microwave observations (collocated with micrometeorological observations for use in future modeling and assimilation studies). The radiometers formed an SSM/I simulator hardened for extended ground-based deployment and capable of long-duration remote operation without frequent absolute calibration. The system robustness was demonstrated over the course of 500 deployed days during REBEX-3 and subsequent experiments.

[65] A custom EASE-Grid software processor was used to generate a data set containing gridded SSM/I satellite brightness observations covering the state of Alaska for the REBEX-3 period. The processor uses the same Backus-Gilbert interpolation routines as the National Snow and Ice Data Center (NSIDC) standard processor. This processor also extracted pixels from all overflights of the REBEX-3 site, including pixels which would have been discarded by the standard processor due to swath overlap.

[66] Very strong linear correlations ($R^2 > 0.92$) between SSM/I EASE-Grid and ground-based brightness observations were found for the 19 and 37 GHz V- and H-polarized channels over the 380 day REBEX-3 period before adjusting for any atmospheric or topographic effects or calibration-related errors. The spread of the points about the best fit line in scatter plots (Figure 9) is consistent with differences in the exact satellite and ground-based observation times during times of day when the microwave brightness changes rapidly. Topographic and atmospheric effects were shown to be small. The residual differences were attributable to errors in the cold calibration of the ground-based observations.

[67] The strength of this linear correlation despite the 4-order-of-magnitude difference in footprint sizes suggests that tundra areas such as the North Slope of Alaska may be well-suited for using the relatively low-resolution satellite microwave brightness observations without disaggregation to estimate surface conditions. This, in turn, is encouraging for a region considered to be a sensitive indicator of climate change as well as for the monitoring of land surface conditions in general.

[68] The comparisons presented in this section were conducted at the 19 and 37 GHz SSM/I frequencies and polarizations because those were the only passive microwave satellite observations available for REBEX-3. Lower-frequency observations with their greater ability to sense through snow and vegetation and into the soil are likely to be more useful for tundra soil-vegetation-atmosphere transfer modeling studies.

[69] Lower-frequency satellite sensors are likely to have a spatial resolution no better than SSM/I, so the gridded REBEX-3 SSM/I data set can give an indication of horizontal homogeneity at the SSM/I sensing depths under various conditions. Also, along with ancillary information on land cover characteristics, this could assist in assessing the effects of subpixel variability at the typically deeper sensing depths of the lower frequencies.

[70] Atmospheric absorption and self-emission, scattering by cloud liquid water droplets and ice crystals, and attenuation and scattering by vegetation would all be less significant at lower microwave frequencies, while at the same time, effective emission depths would be greater. So there would be greater sensitivity to soil conditions at lower frequencies. Atmospheric considerations aside, observations at lower and higher microwave frequencies would provide complementary information about conditions within snow-covered or snow-free soil-vegetation columns simply based on the different effective emission depths.

Appendix A: EASE-Grid Processing Details

[71] In the EASE-Grid implementation, actual SSM/I antenna patterns were used to generate the weighting coefficients for combining swath pixel brightnesses to form interpolated brightnesses. Coefficients were tabulated for interpolation points that form a grid with a density 16 times that of the original swath pixel spacing in the swath reference frame (i.e., a grid spacing of 6.25 km for the 19, 22, and 37 GHz channels and 3.125 km for the 85 GHz channels).

[72] From this densified array the brightness value of the point closest to the center of the desired EASE-Grid cell is reregistered to that EASE-Grid cell location and is used as the brightness value for that cell. This method of assigning interpolated values has two notable features. First, the original swath data are not temporally or spatially averaged as is the case with the ''drop-in-the-bucket'' method used in another SSM/I gridded product (the ''DMSP SSM/I brightness temperature grids'' [*Comiso*, 1990], which cover only polar regions and use 24 hour averaged data). This was a design requirement of the EASE-Grid in order to preserve temporal and spatial fidelity [*Armstrong and Brodzik*, 1995]. Second, the use of a finite-spacing densified grid (rather than interpolating exactly to each EASE-Grid point) provides significant computational efficiencies. The weighting coefficients need be computed only once since the basic SSM/I scan geometry is consistent. The current EASE-Grid processors rely on pretabulated values. For a densified grid spacing of 6.25 km a nominal maximum reregistration distance is $\sim\sqrt{2}/2\times 6.25 = 4.4$ km or 10% of the 19 GHz effective field of view and less than the 10 km maximum geolocation error for swath pixels cited by *Wentz* [1991].

[73] To make the brightness values for the different SSM/I channels represent observations from the same footprints, EASE-Grid standardizes the footprints of all channels to match that of the 19 GHz V-polarized channel. Although the data presented in a ''low-resolution'' EASE-Grid image are displayed on a 25 km grid and the brightness values are depicted with square 25 $\times$ 25 km pixels, the actual resolution of each pixel is that of the 19V channel (43 $\times$ 69 km). NSIDC also processes the 85 GHz swath data into an EASE-Grid product using a 12.5 km grid to retain the higher resolution available from the 85 GHz channels.

[74] The discussion in section 2.2 presented the EASE-Grid as a solution to the problems associated with using nonstationary pixels in a comparison with observations

from fixed points. Through the National Oceanic and Atmospheric Administration/NASA Pathfinder Program, NSIDC produces CD-ROMs containing SSM/I brightness data in EASE-Grid form [*Armstrong et al.*, 1994]. The CD-ROMs for the REBEX-3 period were not available at the time the present comparison study was conducted. Furthermore, even if they had been available, the CD-ROMs would have contained daily images generated from swath data which overlap at high latitudes, resulting in a maximum of two data points for a given Earth location per channel per satellite per day since EASE-Grid discards overlapping pixels rather than averaging them.

[75] This no-averaging choice preserves the temporal fidelity of the SSM/I data. Without it, observations taken hours apart could be combined into a single data point, and any diurnal signal in the observations would be partly filtered out. As mentioned earlier, for locations at the latitude of the REBEX-3 site (69°N), SSM/I observations are made 4–6 times per satellite per day. Since we were interested in examining the satellite observations at the highest possible temporal resolution (to examine diurnal signals, for example), retaining every observation was important.

[76] The preferred solution was to perform EASE-Gridding on one orbit's worth of data at a time, avoiding the overlapping swath problem. NSIDC's operational EASE-Grid processor (referred to here as the "standard" processor) is not configured to operate in this mode. A "custom" EASE-Grid processor was created in cooperation with NSIDC [*Kim et al.*, 1998]. The custom processor splits full orbits into individual ascending and descending orbit segments prior to processing so that no overlapping data is discarded [*O'Kray*, 1998]. For consistency, the core modules which implement the Backus-Gilbert resampling are the exact resampling modules from the standard processor itself.

[77] The TMRS2 85 GHz radiometer experienced temperature control problems during much of the experiment so that the 85 GHz observations are not as accurate as those from the 19 and 37 GHz channels. Furthermore, atmospheric opacity at 85 GHz is several times the opacity at 19 and 37 GHz for identical conditions [*Ulaby et al.*, 1986]. As a result, satellite observations with the 19 and 37 GHz channels more nearly represent surface conditions than do 85 GHz observations. Finally, adding 85 GHz capability to the custom processor would have required substantial extra effort due to the different 12.5 km grid. So, for simplicity, the 85 GHz SSM/I data were not EASE-Gridded.

[78] **Acknowledgments.** We wish to thank the Alaska Department of Transportation as well as colleagues at the Water and Environmental Research Center, University of Alaska, Fairbanks, for their cooperation and assistance.

References

Armstrong, R., and M. Brodzik, An Earth-gridded SSM/I data set for cryospheric studies and global change monitoring, *Adv. Space Res.*, *16*(10), 155–163, 1995.

Armstrong, R. L., K. W. Knowles, M. J. Brodzik, and M. A. Hardman, DMSP SSM/I Pathfinder daily EASE-Grid brightness temperatures [CD-ROM], http://nsidc.org/data/nsidc-0032.html, Natl. Snow and Ice Data Cent., Boulder, Colo., 1994.

Backus, G., and F. Gilbert, Uniqueness in the inversion of inaccurate gross Earth data, *Philos. Trans. R. Soc. London, Ser. A*, *226*, 123–129, 1970.

Chapin, F., and G. Shaver, Individualistic growth response of tundra plant species to environmental manipulations in the field, *Ecology*, *66*, 564–576, 1985.

Chapman, W. L., and J. E. Walsh, Recent variations of sea ice and air temperature in high latitudes, *Bull. Am. Meteorol. Soc.*, *74*, 33–47, 1993.

Comiso, J., DMSPSSM/I daily polar gridded sea ice concentrations, edited by J. Maslanik and J. Stroeve, http://nsidc.org/data/docs/daac/nsidc0002 ssmi seaice.gd.html, Natl. Snow and Ice Data Cent., Boulder, Colo., 1990.

Defense Meteorological Satellite Program, Defense Meteorological Satellite Program DMSP platform document, NASA Marshall Space Flight Cent., Huntsville, Ala., 1995.

Dubois, P., J. van Zyl, and T. Engman, Measuring soil moisture with imaging radars, *IEEE Trans. Geosci. Remote Sens.*, *33*, 915–926, 1995.

England, A., and J. Galantowicz, Moisture in a grass canopy from SSM/I radiobrightness, in *Proceedings of the 2nd Topical Symposium on Combined Optical-Microwave Earth and Atmospheric Sensing*, pp. 12–14, IEEE, Piscataway, N. J., 1995.

Galantowicz, J., Microwave radiometry of snow-covered grasslands for the estimation of land-atmosphere energy and moisture fluxes, Ph.D., thesis, Dep. of Elec. Eng. and Dep. of Atmos. Oceanic and Space Sci., Univ. of Mich., Ann Arbor, 1995.

Galantowicz, J., and A. England, The Michigan Earth grid: Description, registration method for SSM/I data and derivative map projections, *Rep. 027396-2-T*, Univ. of Mich. Radiat. Lab., Ann Arbor, 1991.

Hansen, J., and S. Lebedeff, Global trends of measured surface air temperature, *J. Geophys. Res.*, *92*, 13,345–13,372, 1987.

Henry, G. H. R., and U. Molau, Tundra plants and climate change: The international tundra experiment, *Global Change Biol.*, *3*, 1–10, suppl. 1, 1997.

Hinzman, L. D., and D. L. Kane, Potential response of an Arctic watershed during a period of global warming, *J. Geophys. Res.*, *97*, 2811–2820, 1992.

Hinzman, L., D. Kane, R. Gieck, and K. Everett, Hydrologic and thermal properties of the active layer in the Alaskan arctic, *Cold Reg. Sci. Technol.*, *19*, 95–110, 1991.

Hollinger, J., R. Lo, G. Poe, R. Savage, and J. Pierce, *Special Sensor Microwave/Imager User's Guide*, Nav. Res. Lab., Washington, D.C., 1987.

Hollinger, J., et al., DMSP special sensor microwave/imager calibration/validation final report, Nav. Res. Lab., Washington, D.C., 1989.

Hollinger, J., J. Pierce, and G. Poe, SSM/I instrument evaluation, *IEEE Trans. Geosci. Remote. Sens.*, *28*, 781–790, 1990.

Houghton, J. T., , B. A. Callander, and S. K. Varney (Eds.), *Climate Change 1992: The Supplementary Report to the IPCC Scientific Assessment*, Cambridge Univ. Press, New York, 1992.

Houghton, J. T., B. A. Callander, and S. K. Varney (Eds.), *Climate Change 1995: The Science of Climate Change*, Cambridge Univ. Press, New York, 1996.

Jackson, T., D. LeVine, A. Griffis, D. Goodrich, T. Schmugge, C. Swift, and P. O'Neill, Soil moisture and rainfall estimation over a semiarid environment with the ESTAR microwave radiometer, *IEEE Trans. Geosci. Remote Sens.*, *31*, 836–841, 1993.

Kane, D., R. Gieck, and L. Hinzman, Evapotranspiration from a small Alaskan arctic watershed, *Nord. Hydrol.*, *21*, 253–272, 1990.

Kim, E., and A. England, Radiobrightness thermal inertia sensing of soil and canopy moistures for grassland areas, in *Proceedings of the 2nd Topical Symposium on Combined Optical-Microwave Earth and Atmospheric Sensing*, pp. 39–41, IEEE, Piscataway, N. J., 1995.

Kim, E., et al., A custom EASE-Grid SSM/I processing system, in *International Geoscience and Remote Sensing Symposium Proceedings*, vol. 2, pp. INT.31-02, Seattle, Wash., 1998.

Lachenbruch, A. H., and B. V. Marshall, Changing climate: Geothermal evidence from permafrost in the Alaskan arctic, *Science*, *234*, 689–696, 1986.

Lynch, A., et al., Development of a regional climate model of the western arctic, *J. Clim.*, *8*, 1555–1570, 1995.

Lynch, A., F. Chapin III, L. Hinzman, W. Wu, E. Lilly, G. Vourlitis, and E. Kim, Surface energy balance on the arctic tundra: Measurements and models, *J. Clim.*, *12*, 2585–2606, 1999.

Manabe, S., R. Stouffer, M. Spelman, and K. Bryan, Transient responses of a coupled ocean-atmosphere model to gradual changes of atmospheric CO_2: part I: Annual mean response, *J. Clim.*, *4*, 785–818, 1991.

Michaelson, G., C. Ping, and J. Kimble, Carbon storage and distribution in tundra soils of arctic Alaska, USA, *Arct. Alp. Res.*, *28*, 414–424, 1996.

Oberbauer, S. F., and W. C. Oechel, Maximum CO_2 assimilation rates of vascular plants on an Alaskan arctic tundra slope, *Holarctic Ecol.*, *12*, 312–316, 1989.

Oechel, W. C., and G. Vourlitis, Effect of global change on carbon storage in cold soils, in *Advances in Soil Science: Soils and Global Change*,

edited by R. Lal et al., pp. 117–129, CRC Press, Boca Raton, Fla., 1995.

Oechel, W. C., S. J. Hastings, G. Vourlitis, M. Jenkins, G. Riechers, and N. Grulke, Recent change of arctic tundra ecosystems from a net carbon dioxide sink to a source, *Nature*, *361*, 520–523, 1993.

Oechel, W. C., G. L. Vourlitis, S. J. Hastings, R. C. Zulueta, L. D. Hinzman, and D. L. Kane, Acclimation of ecosystem CO_2 exchange in the Alaskan Arctic in response to decadal climate warming, *Nature*, *406*, 978–981, 2000.

O'Kray, C., TDR to EASE-Grid conversion process documentation, *Rep. RL-960*, Univ. of Mich. Radiat. Lab., Ann Arbor, 1998.

Osterkamp, T. E., and V. E. Romanovsky, Evidence for warming and thawing of discontinuous permafrost in Alaska, *Permafrost Periglacial Processes*, *10*, 17–37, 1999.

Poe, G., Optimum interpolation of imaging microwave radiometer data, *IEEE Trans. Geosci. Remote Sens.*, *28*, 800–810, 1990.

Schanda, E., C. Matzler, and K. Kunzi, Microwave remote sensing of snow cover, *Int. J. Remote Sens.*, *4*, 149–158, 1983.

Schlesinger, W., *Biogeochemistry: An Analysis of Global Change*, Academic, San Diego, Calif., 1991.

Schmugge, T. J., and J.-C. Andre, *Land Surface Evaporation-Measurement and Parameterization*, Springer-Verlag, New York, 1991.

Sellers, P. J., Biophysical models of land surface processes, in *Climate System Modeling*, edited by K. Trenberth, pp. 451–490, Cambridge Univ. Press, New York, 1992.

Seth, A., Land surface heterogeneity in 3-dimensional atmospheric simulations, Ph. D., thesis, Dep. of Atmos. Oceanic, and Space Sci., Univ. of Mich., Ann Arbor, 1995.

Shaver, G. R., Integrated ecosystem research in northern Alaska, in *Landscape Function: Implications for Ecosystem Response to Disturbance: A Case Study in Arctic Tundra*, edited by J. Reynolds and T. Tenhunen, pp. 1947–1993, Springer-Verlag, New York, 1995.

Stogryn, A., Estimates of brightness temperatures from scanning radiometer data, *IEEE Trans. Antennas Propag.*, *26*, 720–726, 1978.

Trenberth, K., (Ed.), *Climate System Modeling*, Cambridge Univ. Press, New York, 1992.

Ulaby, F., R. Moore, and A. Fung, *Microwave Remote Sensing—Active and Passive*, Artech House, Norwood, Mass., 1986.

U.S. Committee on Extension to the Standard Atmosphere (COESA), *U.S. Standard Atmosphere Supplements*, U.S. Govt. Print. Off., Washington, D.C., 1966.

Warren, S., C. Hahn, J. London, R. Chervin, and R. Jenne, Global distribution of total cloud cover and cloud type amounts over land, *NCAR Tech. Note TN-273 + STR*, Natl. Cent. for Atmos. Res., Boulder, Colo., 1986.

Washburn, A. L., and G. Weller, Arctic research in the national interest, *Science*, *233*, 633–639, 1986.

Wentz, F. J., User's manual SSM/I antenna temperature tapes (revision 1), *RSS Tech. Rep. 120191*, Remote Sens. Syst., Santa Rosa, Calif., 1991.

Williams, P. J., and M. W. Smith, *The Frozen Earth: Fundamentals of Geocryology*, Cambridge Univ. Press, New York, 1989.

A. W. England, Department of Atmospheric, Oceanic, and Space Sciences, University of Michigan, EECS 3120, Ann Arbor, MI 48109, USA. (england@umich.edu)

E. J. Kim, Laboratory for Hydrospheric Processes, Code 975, NASA Goddard Space Flight Center, Greenbelt, MD 20771, USA. (Ed.Kim@nasa.gov)